INT. J. REMOTE SENSING, 2002, VOL. 23, NO. 22, 4931–4944

Taylor & Francis
Taylor & Francis Group

GOES-8 and NOAA-14 AVHRR retrieval of smoke aerosol optical thickness during SCAR-B

S. A. CHRISTOPHER*, J. ZHANG

University of Alabama in Huntsville, 320 Sparkman Drive, Huntsville, AL 35806, USA

B. N. HOLBEN

Biospheric Sciences Branch, Code 923, NASA Goddard Space Flight Center, Greenbelt, Maryland, USA

and S.-K. YANG

RDC/Climate Prediction Center/NCEP, Laboratory for Atmospheres, NASA/Goddard Space Flight Center, Greenbelt, Maryland, USA

(*Received 19 March 2001; in final form 22 August 2001*)

Abstract. Using the NOAA-14 1-km Advanced Very High Resolution Radiometer (AVHRR) and the Geostationary Operational Environmental Satellite (GOES-8) imager data, smoke aerosol optical thickness (τ) is retrieved over land during the Smoke, Clouds and Radiation-Brazil (SCAR-B) experiment in Brazil during August–September 1995. The satellite-retrieved τ values are then compared against ground-based sunphotometer derived τ values from the Aerosol Robotic Network (AERONET) program. Both the AVHRR and GOES-8 retrieved τ values are in excellent agreement with the AERONET derived τ values with linear correlation coefficients of 0.93. A single scattering albedo of 0.90 (at 0.67 μm) provides the best fit between the GOES-8 and AERONET τ values. The sensitivity of the retrieved τ to assumed surface albedo and aerosol single scattering albedo are also examined. A simple multi-spectral thresholding algorithm is used to separate smoke from other features from GOES-8 satellite imagery and regional maps of τ are provided. Our results show that the aerosol properties used in this paper are adequate to characterize biomass burning aerosols and can be used in studies that model the role of biomass burning on regional climate.

1. Introduction

Each year more than 100 million tons of smoke aerosols are released into the atmosphere as a result of biomass burning (Hao and Liu 1994). More than 80% of this burning is in the tropical regions and these sub-micron smoke aerosols play a major role on the radiation balance of the earth-atmosphere system (Kaufman *et al.* 1998). They reflect incoming solar radiation back to space, thereby reducing the amount of sunlight reaching the Earth's surface. This is often called the direct effect

*Author for correspondence; e-mail: sundar@nsstc.uah.edu

International Journal of Remote Sensing
ISSN 0143-1161 print/ISSN 1366-5901 online © 2002 Taylor & Francis Ltd
http://www.tandf.co.uk/journals
DOI: 10.1080/01431160110111045

of smoke aerosols (Christopher *et al.* 2000). Current global estimations of the direct radiative forcing range from $-0.1\,\mathrm{Wm}^{-2}$ to $-2.2\,\mathrm{Wm}^{-2}$ (Penner *et al.* 1994), and the uncertainties are attributed to inadequate knowledge of aerosol properties such as chemical composition and the difficulty in properly mapping the spatial distribution of these aerosols. Due to their absorptive nature, smoke aerosols also absorb shortwave radiation thereby heating the atmosphere. The smoke aerosols also serve as cloud condensation nuclei and alter the properties of boundary-layer clouds (Kaufman and Fraser 1997). This effect, called the indirect radiative forcing, is difficult to quantify and has large uncertainties associated with the sign and magnitudes (Hansen *et al.* 1997).

Aerosol optical thickness (τ) is a measure of aerosol loading in the atmosphere (King *et al.* 1999) and is a key parameter that must be carefully measured and studied. Global satellite retrievals of τ are limited to ocean surfaces from NOAA AVHRR data (Stowe *et al.* 1997) and dark targets (Kaufman 1993). Aerosol index can be derived both over land and ocean from the Total Ozone Mapping Spectrometer (TOMS) ultraviolet measurements (Hsu *et al.* 1996). However, it is difficult to obtain aerosol optical depth from the TOMS. Polarization measurements can also be used to derive aerosol information (Deuze *et al.* 1993). Currently, several ground-based sites from the Aerosol Robotic Network (AERONET) program are in operation to obtain τ values (Holben *et al.* 1998). The new generation of GOES imagers (Menzel and Purdom 1994) from geostationary satellites have improved spatial and spectral capabilities that can be used for cloud (Greenwald and Christopher 2000) and biomass burning research (Prins *et al.* 1998, Zhang *et al.* 2001). Although biomass burning fires are routinely studied from GOES imagers (Prins *et al.* 1998), τ information is still unavailable on a routine basis. One distinct advantage of geostationary satellite data is the high temporal resolution when compared to polar orbiting satellites that can be useful in examining the diurnal variation of aerosol optical thickness.

The Smoke, Clouds and Radiation experiment conducted in Brazil (SCAR-B) during August and September 1995 provided comprehensive data sets for understanding the impact of aerosols on the earth-atmosphere system. Kaufman *et al.* (1998) provide a complete review of the measurements and results obtained during SCAR-B. The major goal of this paper is to demonstrate a method for retrieving τ from geostationary (GOES-8) and polar orbiting (NOAA-14 AVHRR) imagers during SCAR-B. The satellite-retrieved τ values are then compared against ground-based sunphotometer values. Using a simple-thresholding method, smoke aerosols are also identified from GOES-8 imagery and regional τ maps are provided.

2. Data sets

Half hourly data from the GOES-8 imager was used. The imager has channels with half-power response bandwidths of $0.52\,\mu\mathrm{m}$–$0.74\,\mu\mathrm{m}$ (channel 1), $3.79\,\mu\mathrm{m}$–$4.04\,\mu\mathrm{m}$ (channel 2), $6.47\,\mu\mathrm{m}$–$7.06\,\mu\mathrm{m}$ (channel 3), $10.2\,\mu\mathrm{m}$–$11.2\,\mu\mathrm{m}$ (channel 4), and $11.6\,\mu\mathrm{m}$–$12.5\,\mu\mathrm{m}$ (channel 5). The effective spatial resolution of channel 1 is $0.57\,\mathrm{km} \times 1\,\mathrm{km}$ and of the other channels is $2.3\,\mathrm{km} \times 4.0\,\mathrm{km}$ (Menzel and Purdom 1994). Channel 1 of the GOES-8 imager was not designed for long-term accurate radiometry and thus has no onboard calibration. All channels of the GOES imagers undergo extensive calibration testing prior to launch (Weinreb *et al.* 1997). However, only the infrared channels (2–5) have onboard calibration. A lack of onboard

calibration for the visible channel makes the reliable retrieval of aerosol optical depth more challenging because calibration errors are one of the largest sources of uncertainty in estimating visible optical depth from satellite radiance measurements (Pincus *et al.* 1997). However, this drawback should not preclude the use of GOES visible channel measurements in aerosol property studies. Other studies have accounted for this degradation and successfully performed cloud property (Greenwald and Christopher 2000, Greenwald *et al.* 1997) and aerosol optical depth (Zhang *et al.* 2001) retrievals.

There have been several recent attempts to assess and monitor the visible channel calibration through vicarious means (e.g. Greenwald *et al.* 1997). These studies report that the GOES-8 imager has undergone signal degradation. The GOES-8 imager visible channel suffered an estimated unexpected drop of about 9% in signal response soon after launch (Ellrod *et al.* 1998). Based on GOES imager measurements of clear ocean scenes, Knapp and Vonder Haar (2000) have estimated the rate of degradation for the GOES-8 imager visible channel to be about 5.6% per year (from August 1995 to August 1999) that is consistent with a simple GOES-8/-9 intercalibration test used by Greenwald *et al.* (1997).

The Advanced Very High Resolution Radiometer (AVHRR) imager data from NOAA-14 consists of measurements from five spectral channels. The five channels are at 0.58 μm–0.68 μm, 0.72 μm–1.1 μm, 3.5 μm–3.9 μm, 10.5 μm–11.5 μm, and 11.5 μm–12.5 μm, respectively. The spatial resolution of this data set is about 1.1 km $\times$ 1.1 km at nadir. The digital counts were converted into top of atmosphere (TOA) albedos through standard calibration procedures. We also account for the degradation of the signal response of the NOAA-14 AVHRR channel using post launch calibration values.

A total of 92 AVHRR LAC images from 16 July to 20 September 1995 between 1600 and 1830 UTC were used in this study. High temporal resolution GOES-8 data from 9 August to 1 September 1995 during the peak of the biomass burning season (Prins *et al.* 1998) were used to examine the diurnal variation of smoke aerosol optical thickness. A total of 127 GOES-8 images between 9 August and 1 September 1995 were used.

The total column τ values were obtained from ground-based sunphotometer measurements (Holben *et al.* 1998). The radiances were measured at 340 nm, 380 nm, 440 nm, 500 nm, 670 nm, 870 nm, and 1020 nm and converted to τ at these seven wavelengths. The τ values used in this paper are obtained after a careful cloud screening process as described in Holben *et al.* (1998). The precision and accuracy of τ estimation could be influenced by various instrumental, calibrational, atmospheric and methodological factors as described in Holben *et al.* (1998). Under cloud-free conditions the total uncertainty in τ from a newly calibrated instrument is $< \pm 0.01$ for $\lambda > 440$ nm and $< \pm 0.02$ for shorter wavelengths (Holben *et al.* 1998).

Figure 1 shows the area of study and an example of biomass burning visible imagery from the NOAA-14 AVHRR for 28 August 1995 at 1800 UTC. Also shown are the locations of selected sunphotometer sites during SCAR-B. Extensive smoke plumes can be seen in the image that is typical of the biomass burning in Brazil. Figure 2 shows hourly GOES-8 images for 28 August 1995 between 1245 and 1945 UTC. The smoke aerosol loading remains high throughout the day. Prins *et al.* (1998) discuss the fire patterns during SCAR-B.

Since the GOES-8 and AVHRR retrieved τ values are compared to the ground-based AERONET data, spatial and temporal collocation is necessary. To spatially

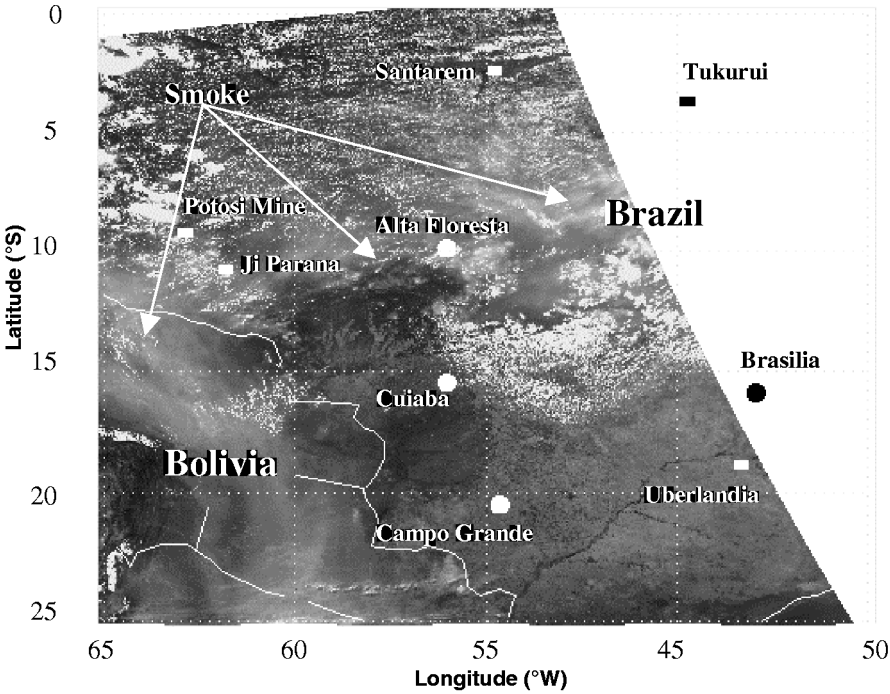

Figure 1. NOAA 14 AVHRR visible image for 28 August 1995 at 1800 UTC. Also shown are the locations of selected sunphotometer sites.

collocate the sunphotometer data with the satellite data, a 3×3 array of GOES-8 (and AVHRR) channel 1 pixels centered on the sunphotometer site was used. This accounts for navigational uncertainties in the satellite data. To temporally collocate the sunphotometer and satellite data, only satellite data within ± 15 minutes of the sunphotometer measurements were used. To minimize cloud contaminated satellite imager pixels, the standard deviation within a 3×3 satellite grid box is examined. If the standard deviation of the collocated channel 1 reflectance values within the 3×3 array of pixels is greater than 0.01, these pixels are rejected as being cloud contaminated. Although this may reject some smoke pixels, this appears to be a stringent test. Note that in this comparison, the sunphotometer data were already checked for cloud contamination using procedures described in Holben *et al.* (1998) and because the satellite data sets have a larger footprint, the additional 3×3 test was used to remove possible cloud contaminated pixels. Tables 1 and 2 show the number of data points used for AVHRR and GOES-8 data sets along with the latitude and longitude of the sunphotometer sites used for the study. Test 1 indicates the number of data points rejected due to lack of temporal collocation between the sunphotometer and the satellite data. Test 2 indicates the number of points rejected due to possible cloud contamination. Only four sites (shown in solid circles in figure 1) were used in the comparison. The other sites (shown in square symbols in figure 1) had insufficient number of data points to perform comparisons against the AERONET data.

3. Methodology and results

The SCAR-B measurements support the assumption that smoke aerosols are well represented by spheres (Martins *et al.* 1998). Therefore Mie calculations were

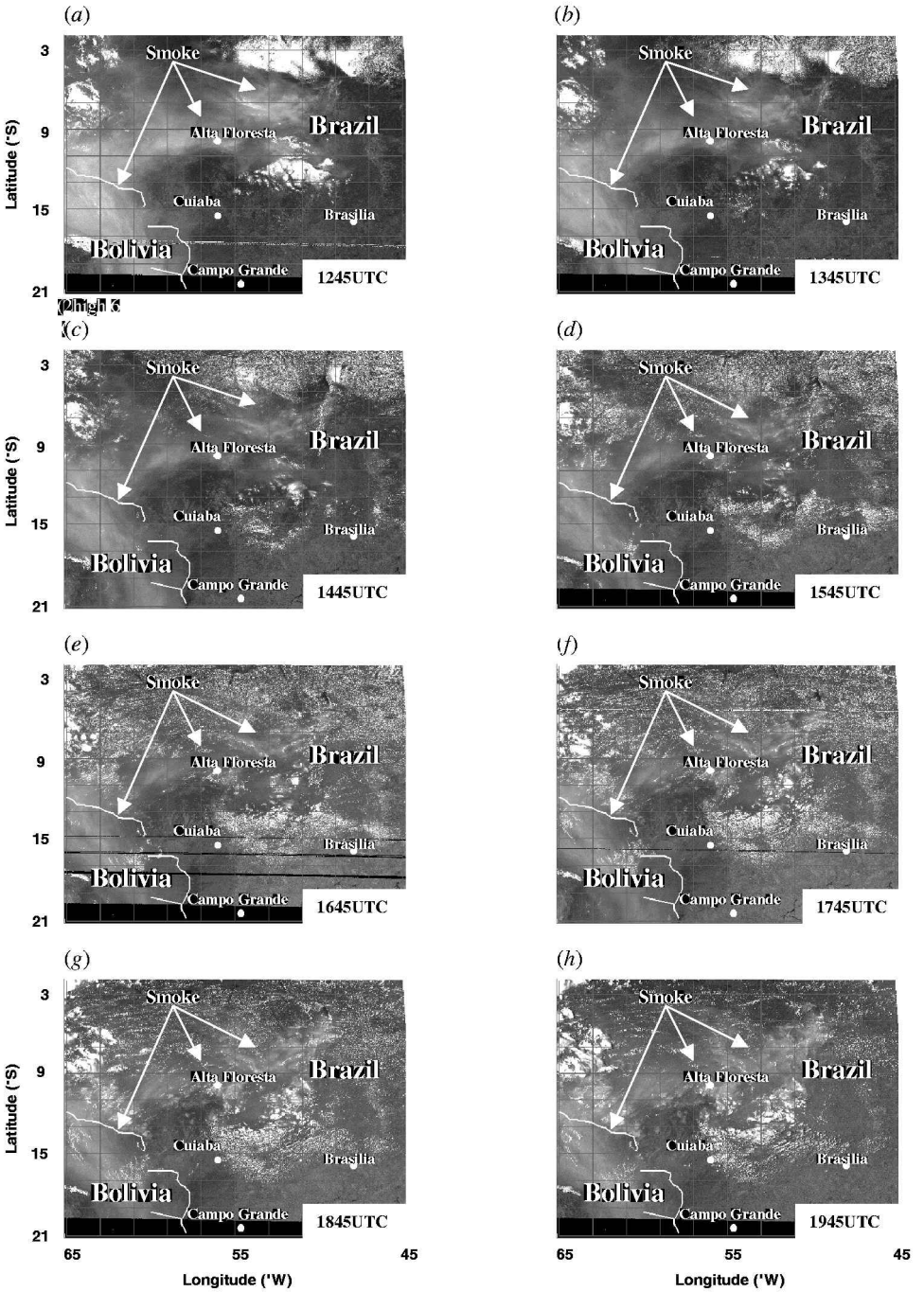

Figure 2. GOES-8 visible image for 28 August 1995 for (*a*) 1245, (*b*) 1345, (*c*) 1445, (*d*) 1545, (*e*) 1645, (*f*) 1745, (*g*) 1845, and (*h*) 1945 UTC.

Table 1. Summary of collocated data between AVHRR and AERONET.

Site	Latitude (°S)	Longitude (°W)	Total points	Test 1	Test 2	Data used
Alta Floresta	9.92	56.0	69	50	4	14*
Brasilia	15.92	47.90	58	19	19	20
Campo Grande	20.45	54.62	74	59	3	12
Cuiaba	15.50	56.00	71	26	8	37

Test 1: Number of points rejected due to lack of temporal within ± 15 min of Sun photometer data.

Test 2: Number of points rejected due to possible cloud contamination (standard deviation of 3×3 AVHRR pixels > 0.01).

*One data point (1640 UTC, 14 September 1995) was rejected because it was out of calculation of look-up-table limit.

Table 2. Summary of collocated data between GOES-8 and AERONET.

Site	Latitude (°S)	Longitude (°W)	Total points	Test 1	Test 2	Data used
Alta Floresta	9.92	56.02	127	64	4	59
Brasilia	15.92	47.90	127	38	43	46
Campo Grande	20.45	54.62	65	38	3	24
Cuiaba	15.50	56.00	127	39	16	72

Test 1: Number of GOES-8 points rejected due to lack of temporal match within ± 15 min of Sun photometer data.

Test 2: Number of GOES-8 points rejected due to possible cloud contamination (standard deviation of 3×3 GOES-8 pixels > 0.01).

performed to obtain the scattering and absorbing properties of aerosols. The biomass burning aerosols are characterized as an internal mixture of black carbon core surrounded by an organic shell (Zhang *et al.* 2001). A lognormal size distribution is assumed with an average volume mean diameter of 0.3 μm and a standard deviation of 1.8 (Reid *et al.* 1998). The densities of the black carbon core and the organic shell were assigned values of 1.8 gcm^{-3} and 1.2 gcm^{-3} respectively (Ross *et al.* 1998). The real part of the refractive index of the shell ranges from 1.4 to 1.6 (Martins *et al.* 1998). Therefore, for the organic shell, a mean value of 1.5 was used with no absorption (Ross *et al.* 1998). The real and imaginary part of the refractive index of the black carbon core is assumed to be 1.63i–0.48i (Chang and Charamampoulos 1990). In this study, the mass fraction of the black carbon core is assumed to 4.5%, which is well within the range of previous studies (Pereira *et al.* 1996, Ferek *et al.* 1998, Artaxo *et al.* 1998). This yielded a single scattering albedo (ω_0) of 0.90 at 0.67 μm. One of the key parameters that affects optical thickness retrievals is ω_0 (Chu *et al.* 1998, Zhang *et al.* 2001). Therefore, the sensitivity of the retrieved τ to ω_0 is examined by varying the mass fraction of the black carbon core to yield different values of ω_0. A mass fraction of 3% yielded a value of 0.93 and a mass fraction of 6% yielded a value of 0.87.

The scattering and absorption properties from the Mie calculations are then used in a discrete ordinate radiative transfer (DISORT) model (Ricchiazzi *et al.* 1998) to pre-calculate the satellite measured spectral radiance as a function of τ, sun-satellite viewing geometry and surface albedo (Zhang *et al.* 2001). Therefore, for a given

satellite visible channel radiance and a known sun-satellite view geometry, an optical thickness value can be obtained from the pre-computed tables. Values of surface albedo are also required for simulating the satellite observed radiance. A Lambertian surface is assumed and surface reflectivity is obtained by calculating the minimum top of atmosphere (TOA) radiance over the study period. The mean surface reflectance values from the GOES-8 imager for the AERONET sites where retrievals were performed are as follows; 0.084 ± 0.007 (AltaForesta), 0.080 ± 0.010 (Brasilia), 0.110 ± 0.010 (Campo Grande) and 0.082 ± 0.005 (Cuiaba).

Figure 3a shows the relationship between GOES-8 and AERONET retrieved τ for the entire study period. A total of 201 points were used. Data for all four sites are shown in different symbols and the results are summarized in table 3. Also shown for each point are the standard deviation in time (along the abscissa, ± 15 min) and space (along the ordinate, 3×3 box). The inset of figure 3a also shows the frequency distribution of τ for both the GOES-8 and AERONET data. There is excellent agreement between the GOES-8 and AERONET derived τ values with linear correlation coefficient of 0.93. The dashed line in figure 3a denotes the one to one fit and the solid line is the linear regression fit through the points. There is a large scatter in the data points when τ is low ($\tau < 0.1$) when compared with large optical thickness values which shows the difficulty in estimating in retrieving τ over land from satellite measurements when τ is low. Table 3 shows the linear correlation coefficient (R), the slope and intercept for each site for the entire study period. Also shown are the mean and standard deviations of τ for each site. The correlation is high between the AERONET and GOES-8 retrieved τ values for Alta Foresta and Cuiaba with the lowest correlation for Brasilia. This is because mean τ values are very low in Brasilia (0.05 ± 0.02). Figure 3b shows similar results between AVHRR and AERONET retrieved τ and table 4 summarizes the results. Again, the correlation is high for AltaForesta, Campo Grande and Cuiaba. However, overall correlation coefficients between AVHRR and AERONET is 0.93 and between GOES-8 and AERONET is 0.93.

Next we estimate the uncertainty in the optical thickness retrieval due to changes in ω_0, surface albedo (α_{sfc}) and degradation in signal response of the GOES-8 visible channel. Table 5 shows the change in τ due to $\pm 10\%$ change in signal degradation, during 1995, of the GOES-8 visible channel and a $\pm 10\%$ change in α_{sfc}. Also shown is the sensitivity of the optical thickness results to a change in ω_0 from 0.87 to 0.93, which is well within the range of SCAR-B measurements (Reid *et al.* 1998). The τ retrievals are sensitive to assumed values of ω_0 at large τ values. For example, when the GOES-8 τ is 1.0 (retrieved with an ω_0 of 0.90), roughly corresponding to the mean τ over Alta Foresta, a $\pm 3\%$ change in ω_0 (0.90 ± 0.03) produces roughly a 25% change in τ (1.0 ± 0.3). However, at small optical thickness ($\tau = 0.25$), a $\pm 3\%$ change in ω_0 (0.90 ± 0.03) produces only a 12% change in τ (0.25 ± 0.03). The uncertainty in retrieved τ values due to the assumed α_{sfc} is large for smaller τ when compared to large τ because the satellite receives reflected radiation not only from the aerosol layer but also the surface. For example when the GOES-8 τ is 0.25 (retrieved with an ω_0 of 0.90), a $\pm 10\%$ change in α_{sfc} ($0.08 \pm 10\%$), corresponding to the mean cloud-free surface reflectance over Cuiaba, produces a 28% change in τ (0.25 ± 0.07). Table 5 shows that for small τ values the uncertainties in the retrieved τ values are larger due to different α_{sfc} values. As τ increases, the satellite 'sees' less of the surface and therefore the uncertainties in τ retrieval decreases. For a unit τ value, a $\pm 10\%$ change in signal degradation produces about 25% change in

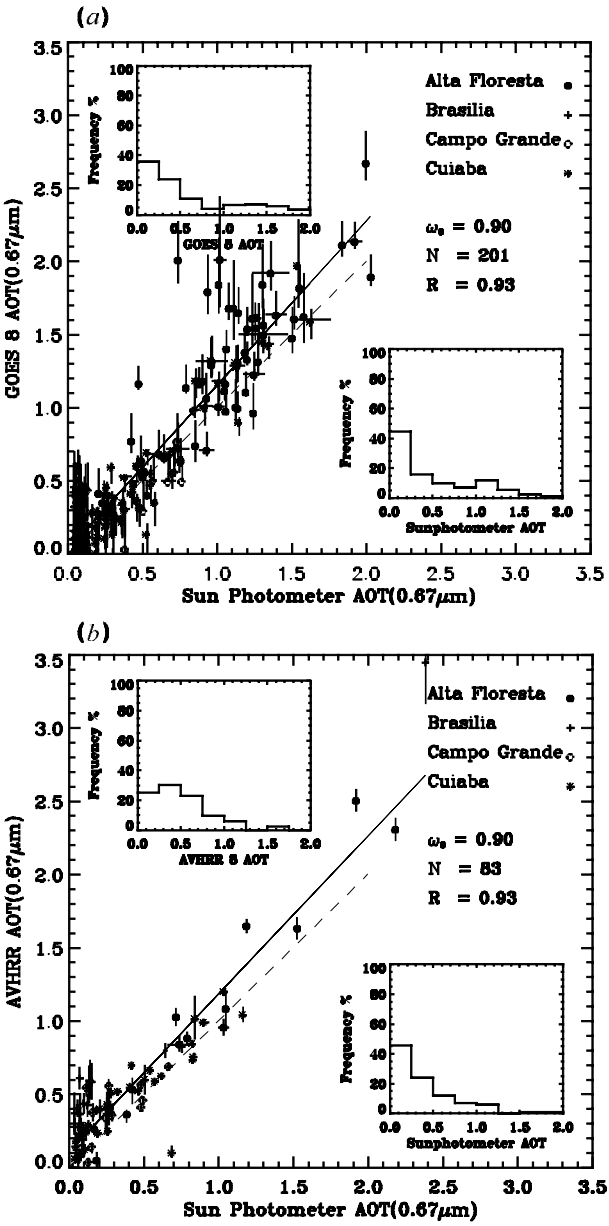

Figure 3. Aerosol optical thickness (AOT) for four sunphotometer sites in Brazil during SCAR-B, (a) GOES-8 vs. AERONET and (b) NOAA-14 AVHRR vs AERONET. Also shown in the inset is the frequency distribution of GOES-8 and AERONET retrieved aerosol optical thickness.

τ (1.0 ± 0.22). As τ increases, the uncertainties due to degradation increase also because a larger τ corresponds to a high GOES-8 visible channel reflectance. A small change in visible reflectance at large τ produces a large change in retrieved τ values. To minimize errors for small optical thickness regimes, accurate surface albedo values are needed. This is the main reason that the GOES-8 optical thickness values over

Table 3. Summary of results for the study period for GOES-8 data.

Site	Number of points	GOES-8 τ		AERONET τ		R	Slope	Intercept	ω_0 (0.67 μm)
		μ	σ	μ	σ				
Alta Floresta	59	1.26	0.52	1.04	0.41	0.81	1.01	0.21	0.90
Brasilia	46	0.12	0.15	0.05	0.02	0.16	1.36	0.04	0.90
Campo Grande	24	0.33	0.25	0.30	0.27	0.67	0.71	0.07	0.90
Cuiaba	72	0.46	0.45	0.44	0.38	0.94	0.80	0.07	0.90
Total/mean	201	0.60	0.60	0.51	0.50	0.93	1.13	0.03	

R denotes linear correlation coefficient, and μ and σ denote the mean and standard deviation respectively.

Table 4. Summary of results from the study period for NOAA-14 AVHRR.

Site	Number of points	AVHRR τ		AERONET τ		R	Slope	Intercept	ω_0 (0.67 μm)
		μ	σ	μ	σ				
Alta Floresta	14	1.25	0.96	1.05	0.72	0.97	1.30	−0.11	0.90
Brasilia	20	0.34	0.18	0.10	0.07	0.41	0.99	0.23	0.90
Campo Grande	12	0.45	0.22	0.36	0.23	0.76	0.73	0.19	0.90
Cuiaba	37	0.47	0.31	0.39	0.31	0.89	0.87	0.13	0.90
Total	83	0.57	0.55	0.43	0.48	0.93	1.08	0.10	0.90

R denotes linear correlation coefficient, and μ and σ denote the mean and standard deviation respectively.

Table 5. Sensitivity of retrieved aerosol optical thickness to GOES-8 signal degradation, surface albedo (α_{sfc}) and single scattering albedo (ω_0).

TAU (0.67 μm)	Degradation		α_{sfc}		ω_0	
	−10%	+10%	−10%	+10%	0.87	0.93
0.25	0.18	0.33	0.32	0.18	0.28	0.22
0.50	0.38	0.63	0.57	0.43	0.59	0.43
0.75	0.59	0.95	0.81	0.68	0.93	0.64
1.00	0.78	1.28	1.06	0.93	1.30	0.83
1.25	0.98	1.62	1.31	1.19	1.70	1.02
1.50	1.18	1.97	1.55	1.44	2.13	1.19
1.75	1.37	2.33	1.80	1.69	2.60	1.36
2.00	1.56	2.71	2.04	1.94	3.09	1.52

Brasilia do not agree well with the AERONET values. One way to reduce this uncertainty is to obtain surface albedo for each time period rather than an average value for an entire day. We therefore obtained clear sky estimates for three time periods (1145, 1445 and 1745 UTC) and used these values in the retrieval process. The absolute error decreased from 0.14 to 0.10. We also tested the sensitivity of the retrieved aerosol optical thickness due to different aerosol vertical profiles. Our results indicate that the retrieved aerosol optical thickness is not very sensitive at 0.67 μm, partly due to the low Rayleigh scattering. In summary, the two major effects on aerosol optical thickness retrievals are the α_{sfc} and ω_0. These two factors tend to

work in opposite directions. For small τ values the effect of α_{sfc} is larger than that of ω_0. This is reversed for large optical thickness. However, our results indicate that an ω_0 of 0.90 can be used to characterize biomass burning aerosols that confirms the results of Chu *et al.* (1998) and Zhang *et al.* (2001). With better quality satellite imagers, the degradation in signal response could become less of a problem.

Next we show some preliminary results of τ retrievals over the study area from the GOES-8 imager. Each GOES-8 imager pixel is classified as cloudy or cloud-free pixels. The cloud-free pixels contain both smoke aerosols and clear-sky pixels. The basic idea is to first obtain clear sky (or background values). Then smoke and cloudy pixels are identified if the measured values are greater than the background values by a certain threshold. The background values for channel 1 of the GOES-8 imager are obtained by assuming that the lowest channel 1 reflectances over the study period corresponds to clear sky values ($\rho_{0.63\ clear}$). Similarly clear sky values for the reflectance portion of channel 2 ($\rho_{3.9\ clear}$) is obtained by calculating the lowest reflectances over the study period (Christopher *et al.* 2000). Then a gross cloud check is performed by removing all pixels with cloud top temperatures colder than 273 K and with channel 1 reflectances greater than 35% ($\rho_{0.63} > 0.35$ and $T_{10.7} < 273$ K). This leaves the image with smoke aerosols and clouds with cloud top temperatures warmer than 273 K. Next, cumulus clouds were removed from the image if the standard deviation of a 3×3 box in the visible channel was greater than 0.02 and if $(\rho_{0.63} - \rho_{0.63clear}) > 0.05$. Clouds are now separated from smoke aerosols by using the $\rho_{3.9}$ information. Smoke aerosols due to their small sizes are nearly transparent at these wavelengths (Kaufman and Fraser 1997; Christopher *et al.* 2000) whereas clouds with water droplets scatter the incoming solar radiation based on their particle size (Greenwald and Christopher 2000). Using this information, further cloud screening is done if the following criteria are satisfied: $(\rho_{0.63} - \rho_{0.63clear}) > 0.05$ and $(\rho_{3.9} - \rho_{3.9\ clear}) > 0.03$. The first criteria identify pixels as cloudy if the difference between the clear and measured channel 1 reflectance is greater than 5%. The second threshold assumes that for cloudy pixels, water clouds have a difference in channel 2 reflectivity between measured and clear sky values of 3%. We inspected the quality of the smoke identification method by examining the images visually. The algorithm appears to be well suited to remove clouds from satellite imagery. However, cloud edges sometimes pose problems by being classified as smoke aerosols.

Figure 4 shows the smoke aerosol optical thickness for the study area. The corresponding visible channel images are shown in figure 2. Figure 4 shows that the heaviest aerosol loading for this particular day is around 1245 UTC around 64 W and 14 S and the aerosol loading continues to decrease as the day progresses. The frequency of cumulus clouds increases and at 1945 UTC, the smoke aerosol loading decreases. These images show that the method used to separate smoke from clouds and clear sky works well. These optical thickness maps can be used to calculate the diurnal variation of the radiative effects of biomass burning aerosols.

Figure 5 shows the daytime diurnal variation of smoke aerosol optical thickness for August 1995 over Cuiaba from GOES-8, AVHRR and AERONET data. Aerosol optical thickness over Cuiaba is high during the first two weeks of August and values continue to decrease towards the end of the month. The GOES and AVHRR derived τ values agree well with the AERONET values. Even though a fixed ω_0 value of 0.90 was used, the GOES-8 diurnal variation compare well with the AERONET retrievals. The GOES and AVHRR values are also consistent with one another. The mean daytime diurnal variation is 0.46 ± 0.45 and 1.26 ± 0.52 over Cuiaba and Alta Foresta for the study period indicating high aerosol loading.

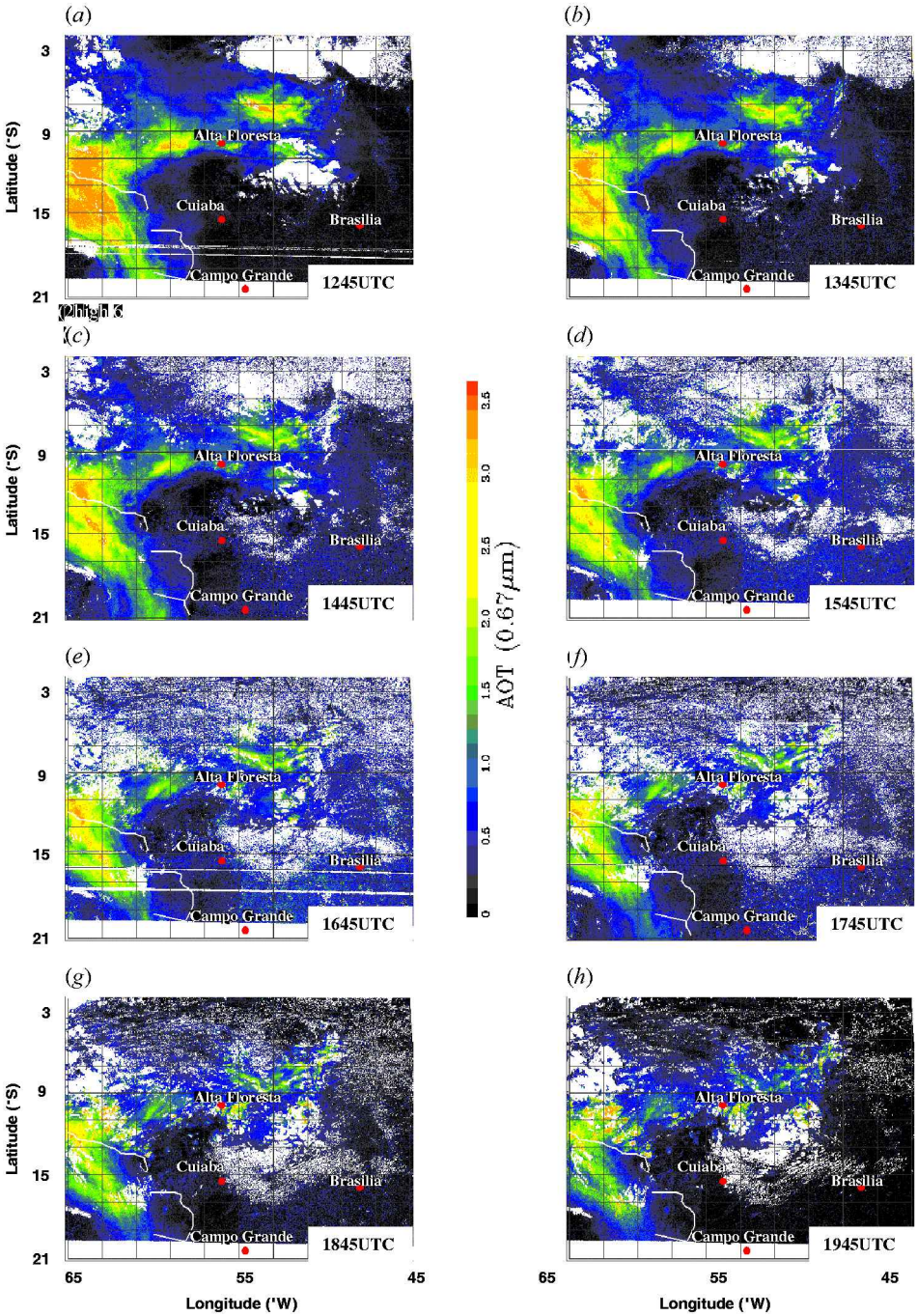

Figure 4. Example of spatial distribution of smoke aerosol optical thickness for 24 August 1998 from GOES-8 imagery for same time periods as figure 2.

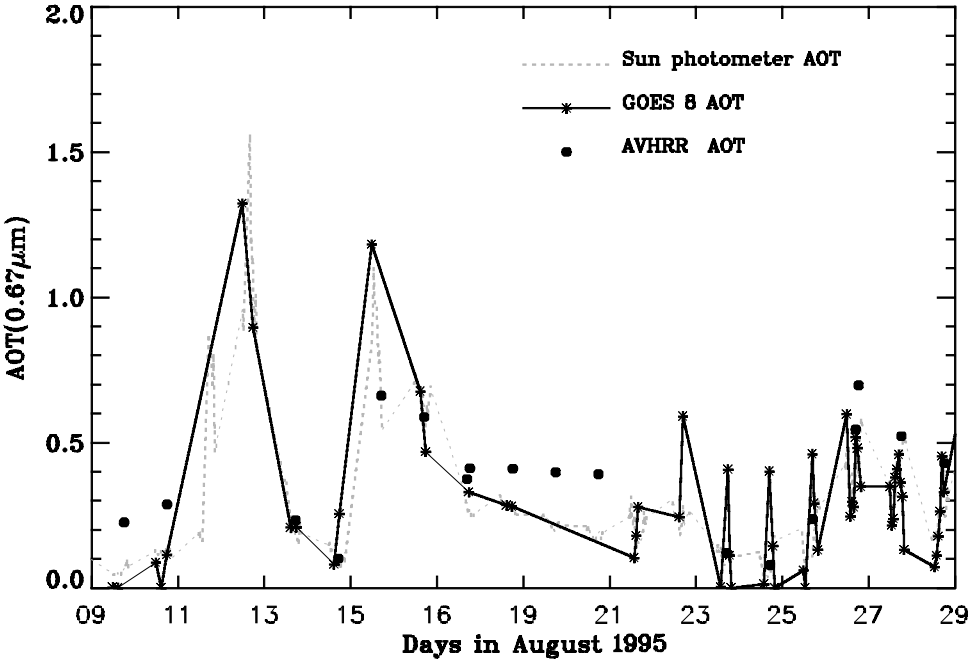

Figure 5. Diurnal variation of smoke aerosol optical thickness (AOT) from GOES-8 for the study period for Cuiaba. Also superimposed are the AVHRR retrieved and AERONET values.

4. Summary

Using a polar orbiting satellite (NOAA-14) imager (AVHRR) and a geostationary imager (GOES-8) aerosol optical thickness is retrieved during the Smoke Clouds and Radiation Experiment—Brazil (SCAR-B). The satellite-retrieved τ values are compared against ground-based τ values for four AERONET sites. Using a set of visible, near-infrared and infrared thresholds, clouds are removed from GOES-8 imagery and τ is retrieved over the entire study area. Our results indicate that both the AVHRR and GOES retrieved τ values are in excellent agreement with AERONET values. The single scattering albedo used for these calculations are 0.90 (at 0.67 μm) that appears to be the growing consensus for characterizing biomass burning aerosols in radiative transfer calculations (Chu *et al.* 1998; Zhang *et al.* 2001). These results can be used to test models that simulate smoke aerosol optical thickness.

Acknowledgements

This research was supported in part by NASA's Global Aerosol Climatology Project (NCC-8141) and NASA'S IDS project (Flame and Biomass Burning Experiment, FLAMBE).

References

Artaxo, P. E., Fernandes, T., Martins, J. V., Yamasoe, M. A., Hobbs, P. V., Maenhaut, W., Longo, K. M., and Castanho, A., 1998, Large-scale aerosol source apportionment in Amazonia. *Journal of Geophysical Research*, **103**, 31837–31847.

Chang, H., and Charalampopoulos, T. T., 1990, Determination of the wavelength dependence of refractive indices of flame soot. *Proceedings of the Royal Society of London*, **430**, 577–591.

Christopher, S. A., Chou, J., Zhang, J., Li, X., and Welch, R. M., 2000, Shortwave direct radiative forcing of biomass burning aerosols estimated from VIRS and CERES. *Geophysical Research Letters*, **27**, 2197–2200.

Chu, D. A., Kaufman, Y. J., Remer, L. A., and Holben, B. N., 1998, Remote sensing of smoke from MODIS airborne simulator during the SCAR-B experiment. *Journal of Geophysical Research*, **103**, 31979–31987.

Deuze, J. L., Breon, F. M., Deschamps, P. Y., Devaux, C., Herman, M., Podaire, A., and Roujean, J. L., 1993, Analysis of the POLDER (Polarization and Directionality of Earth's Reflectances) airborne instrument observations over land surface. *Remote Sensing of Environment*, **45**, 137–154.

Ellrod, G. P., Achutnui, R. V., Daniels, J. M., Prins, E. M., and Nelson, J. P., 1998, An assessment of GOES-8 imager data quality. *Bulletin of the American Meteorological Society*, **78**, 1971–1983.

Ferek, R. J., Reid, J. S., Hobbs, P. V., Blake, D. R., and Liousse, C., 1998, Emission Factors of hydrocarbons, halocarbons, trace gases, and particles from biomass burning in Brazil. *Journal of Geophysical Research*, **103**, 32 107–32 118.

Greenwald, T. J., and Christopher, S. A., 2000, The GOES-IM Imagers: New Tools for studying the microphysical properties of boundary layers clouds. *Bulletin of the American Meteorological Society*, **81**, 2607–2620.

Greenwald, T. J., Christopher, S. A., and Chou, J., 1997, Cloud liquid water path comparisons from passive microwave and solar reflectance satellite measurements: Assessment of sub-field-of-view cloud effects in microwave retrieval. *Journal of Geophysical Research*, **102**, 19585–19597.

Hao, W. M., and Liu, M. H., 1994, Spatial and temporal distribution of biomass burning. *Global Biogeochemical Cycles*, **8**, 495–503.

Hansen, J., Sato, M., Lacis, A., and Ruedy, R., 1997, The missing climate forcing. *Transactions of the Royal Society of London*, **352**, 231–240.

Holben, B. N., Eck, T. F., Slutsker, I., Tanre, D., Buis, J. P., Setzer, A., Vermote, E., Reagan, J. A., Kaufman, Y. J., Nakajima, T., Lavenu, F., Jankowiak, I., and Smirnov, A., 1998. AERONET—A Federated Instrument Network and Data Archive for Aerosol Characterization. *Remote Sensing of Environment*, **66**, 1–16.

Hsu, N. C., Herman, J. R., Bhartia, P. K., Seftor, C. J., Torres, O., Thompson, A. M., Gleason, J. F., Eck, T. F., and Holben, B. N., 1996. Detection of biomass burning smoke from TOMS measurements. *Geophysical Research Letters*, **23**, 745–748.

Kaufman, Y. J., 1993, Measurements of the aerosol optical thickness and the path radiance —Implications on aerosol remote sensing and atmospheric corrections. *Journal of Geophysical Research*, **98**, 2677–2692.

Kaufman, Y. J., and Fraser, R. S., 1997, Confirmation of the smoke particles effect on cloud and climate. *Science*, **277**, 1636–1639.

Kaufman, Y. J., Hobbs, P. V., Kirchoff, V. W., Artaxo, P., Remer, L. A., Holben, B. N., King, M. D., Prins, E. M., Ward, D .E., Longo, K. M., Mattos, L. F., Nobre, C. A., Spinhirne, J. D., Ji, Q., Thompson, A. M., Gleason, J. F., Christopher, S. A., and Tsay, S. C., 1998, The Smoke, Clouds and Radiation Experiment in Brazil (SCAR-B). *Journal of Geophysical Research*, **103**, 31783–31808.

King, M. D., Kaufman, Y. J., Tanre, D., and Nakajima, T., 1999, Remote Sensing of Tropospheric Aerosols from Space: Past, Present and Future. *Bulletin of American Meteorological Society*, **80**, 2229–2287.

Knapp, K., and Vonder Haar, T., 2000, Calibration of the eighth Geostationary Operational Environmental Satellite (GOES-8) Imager Visible Sensor. *Journal of Atmospheric and Oceanic Technology*, **17**, 1639–1644.

Martins, J. V., Hobbs, P. V., Weiss, R. E., and Artaxo, P., 1998, Sphericity and morphology of smoke particles from biomass burning in Brazil. *Journal of Geophysical Research*, **103**, 32051–32058.

Menzel, W. P., and Purdom, J. F. W., 1994, Introducing GOES-I: The first of a new generation of Geostationary Operational Environmental Satellites. *Bulletin of American Meteorological Society*, **75**, 757–781.

Penner, J. E., Charlson, R. J., Hales, J. M., Laulainen, N. S., Leifer, R., Novakov, T., Ogren, J., Radke, L. F., Schwartz, S. E., and Travis, L., 1994, Quantifying and

minimizing uncertainty of Climate Forcing by Anthropogenic Aerosols. *Bulletin of the American Meteorological Society*, **75**, 375–400.

Pereira, E. B., Setzer, A. W., Gerab, F., Artaxo, P. E., Pereira, M. C., and Monroe, G., 1996, Airborne measurements of aerosols from burning biomass in Brazil related to the TRACE A experiment. *Journal of Geophysical Research*, **101**, 23983–23992.

Pincus, R., Baker, M. A., and Bretherton, C. S., 1997, What controls stratocumulus radiative properties? Lagrangian observations of cloud evolution. *Journal of Atmospheric Science*, **54**, 2215–2236.

Prins, E. M., Feltz, J. M., Menzel, W. P., and Ward, D. E., 1998, An overview of GOES-Diurnal Fire and Smoke Results for SCAR-B and the 1995 Fire Season in South America. *Journal of Geophysical Research*, **103**, 31821–31,836.

Reid, J. S., Hobbs, P. V., Ferek, R. J., Blake, D. R., Martins, J. V., Dunlap, M. R., and Liousse, C., 1998, Physical, chemical and optical properties of regional hazes dominated by smoke in Brazil. *Journal of Geophysical Research*, **103**, 32059–32080.

Ricchiazzi, P., Yang, S., Gautier, C., and Sowle, D., 1998, Sbdart: A Research and Teaching Software Tool for Plane-Parallel Radiative Transfer in the Earth's Atmosphere. *Bulletin of the American Meteorological Society*, **79**, 2101–2114.

Ross, J. L., Hobbs, P. V., and Holben, B., 1998, Radiative characteristics of regional hazes dominated by smoke from biomass burning in Brazil: Closure tests and direct radiative forcing. *Journal of Geophysical Research*, **103**,31925–31941.

Stowe, L. L., Ignatov, A. M., and Singh, R. R., 1997, Development, validation, and potential enhancements to the second-generation operational aerosol product at the National Environmental Satellite, Data, and Information Service of the National Oceanic and Atmospheric Administration. *Journal of Geophysical Research*, **102**, 16923–16934.

Weinreb, M. P., Jamison, M., Fulton, N., Chen, Y., Johnson, J. X., Bremer, J., Smith, C., and Baucum, J., 1997, Operational calibration of Geostationary Operational Environmental Satellite-8 and -9 imagers and sounders, *Applied Optics*, **36**, 6895–6904.

Zhang, J., Christopher, S. A., and Holben, B., 2001. Intercomparison of aerosol optical thickness derived from GOES-8 Imager and Ground-Based Sun Photometers. *Journal of Geophysical Research*, **106**, 7387–7397.